Numerical study of pressure forcing of wind on dynamically evolving water waves

Yi Liu, Di Yang, Xin Guo, and Lian Shen[a)]
Department of Civil Engineering, Johns Hopkins University, Baltimore, Maryland 21218, USA

(Received 4 January 2010; accepted 6 April 2010; published online 30 April 2010)

We simulate the dynamic evolution of nonlinear water waves coupled with wind turbulence. We first investigate simple wave trains to obtain pressure distribution, based on which parameters for wave growth are quantified and their dependence on wave age and wave steepness is shown. We then investigate broadband waves to obtain physical insights to wind forcing for phase-resolved wavefield simulation. It is found that for long wave components, the wave growth parameter can be approximated by the value of the corresponding monochromatic waves; for short waves, stochastic modeling is suggested. © *2010 American Institute of Physics*. [doi:10.1063/1.3414832]

The accurate prediction of ocean surface waves is important to many applications in ocean science and engineering. The evolution of wavefield is affected mainly by nonlinear wave interaction, wind forcing, and wave breaking dissipation. The majority of existing wave prediction tools simulate the evolution of directional wave spectrum. The information of wave phases is not contained in the wave spectrum, and the aforementioned three processes are parametrized in a phase-averaged context.[1]

To obtain a more direct description of the wavefield with finely resolved spatial and temporal details, it is desirable to resolve the wave phases in the simulation. Such information will be valuable for the mechanistic study of wind-wave dynamics which may eventually lead to improved modeling for the wave spectrum simulation. Recent advancement in computing power and algorithm development has facilitated the phase-resolved simulation of nonlinear wave interaction involving a large number of wave modes [e.g., $O(10^4)$ modes in each direction as shown by Wu[2]]. Central to the development is an efficacious high-order spectral (HOS) method that is capable of directly capturing nonlinear wave interaction at a reasonable computational cost. The HOS method directly simulates the evolution of surface elevation η and surface potential Φ^s, which is defined as the surface value of the velocity potential Φ. With a perturbation series of Φ with respect to the wave steepness to the order of M and Taylor series expansion about the mean water level $z=0$,

$$\Phi(x,y,z,t)=\sum_{m=1}^{M}\Phi^{(m)}(x,y,z,t),$$
$$\Phi^s(x,y,t)=\sum_{m=1}^{M}\sum_{l=0}^{M-m}\frac{\eta^l}{l!}\frac{\partial^l\Phi^{(m)}}{\partial z^l}\bigg|_{z=0}, \tag{1}$$

and an eigenfunction expansion of each $\Phi^{(m)}$ with N modes,

$$\Phi^{(m)}(x,y,z,t)=\sum_{n=1}^{N}\Phi_n^{(m)}(t)\Psi_n(x,y,z),\quad z\le 0, \tag{2}$$

the kinematic and dynamic free surface boundary conditions are written as[3]

$$\frac{\partial\eta}{\partial t}=-\nabla_h\eta\cdot\nabla_h\Phi^s+(1+|\nabla_h\eta|^2)\times\left[\sum_{m=1}^{M}\sum_{\ell=0}^{M-m}\frac{\eta^\ell}{\ell!}\sum_{n=1}^{N}\Phi_n^{(m)}(t)\ \frac{\partial^{\ell+1}\Psi_n(x,y,z)}{\partial z^{\ell+1}}\bigg|_{z=0}\right], \tag{3}$$

$$\frac{\partial\Phi^s}{\partial t}=-g\eta-\frac{1}{2}|\nabla_h\Phi^s|^2+D_\Phi-\frac{p_a(x,y,t)}{\rho_w}+\frac{1}{2}(1+|\nabla_h\eta|^2)\times\left[\sum_{m=1}^{M}\sum_{\ell=0}^{M-m}\frac{\eta^\ell}{\ell!}\sum_{n=1}^{N}\Phi_n^{(m)}(t)\frac{\partial^{\ell+1}\Psi_n(x,y,z)}{\partial z^{\ell+1}}|_{z=0}\right]^2. \tag{4}$$

Here, $\nabla_h\equiv(\partial/\partial x,\partial/\partial y)$ is the horizontal gradient, D_Φ is the wave dissipation, p_a is the atmospheric pressure at the wave surface, ρ_w is the density of water, and g is the gravitational acceleration. By using a pseudospectral method, the HOS method accounts for the nonlinear interactions among all the N wave modes up to the desired perturbation order M in wave steepness, with a computational cost proportional to $MN\ln N$. Complete review of the HOS method is provided in Chap. 15 of Mei *et al.*[4]

While the HOS method provides a vehicle for the nonlinear wave simulation in a phase-resolved framework, the wave breaking dissipation D_Φ and the wind forcing p_a remain to be specified in a phase-resolved context. The model development for these terms is still at an early stage, and this letter investigates the characteristics of p_a.[5–11] For this purpose, we perform coupled simulations of wind turbulence and wave evolution (Fig. 1). To our best knowledge, this is the first simulation-based study that addresses the two-way dynamical coupling between wind and narrowband/broadband waves with all of the essential nonlinear wave interaction processes being resolved to high order. (We note that recently a powerful numerical capability has been developed for the large-scale simulation of air-water coupled

a)Author to whom correspondence should be addressed. Electronic mail: lianshen@jhu.edu.

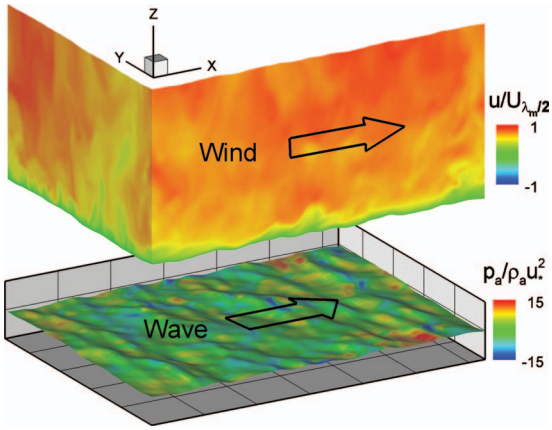

FIG. 1. (Color) Illustration of wind turbulence and water wave coupled simulation. Plotted are streamwise velocity (normalized by $U_{\lambda_m/2}$) of the wind and pressure (normalized by $\rho_a u_*^2$) distribution on the surface of broadband waves ($c_m/u_*=12.3$). The air domain is lifted up for better visualization.

flows including wind-driven waves on top-ranked supercomputers such as the Earth Simulator.[12]) For wind over simple wave trains, we use direct numerical simulation (DNS) for wind turbulence. The approach of DNS has been proven to faithfully capture the pressure variation in wind over water waves.[9,11,13] For broadband waves, in order to resolve the wind-wave interaction over a wide range of wavenumbers, we use large-eddy simulation (LES).

For the wind simulation, we consider as a canonical problem Couette air flow over water waves. We simulate the Navier–Stokes equations for the air motion on a time-dependent boundary-fitted grid. For spatial discretization, we use a hybrid pseudospectral and finite-difference scheme. Time integration of the momentum equation is realized through a fractional step scheme. Details of the numerical scheme and the validation using the data in the literature[7–11] are provided by Refs. 13–15.

Different from Refs. 13 and 14 where the waves do not evolve dynamically, in this letter the wind turbulence simulation is dynamically coupled with the HOS wave simulation through a fractional step method with two-way feedbacks. At the subtimesteps, the HOS simulation provides the wind simulation with the wave surface geometry and the normal and tangential surface velocities as the Dirichlet boundary conditions; the windfield evolves dynamically, subject to the wave form and friction drags that are generated naturally from the retardance by the wave calculated by the HOS simulation; the wind simulation provides $p_a(x,y,t)$ on the wave surface, which the HOS simulation uses as the wind forcing in Eq. (4) to advance the wave in time. After the above coupling, the entire wind-and-wave field advances to the next timestep. The numerical details of the dynamic coupling are provided by Yang.[15]

We discuss simple wave trains first. Note that the wave is initially monochromatic. Due to nonlinear wave interaction and the excitation by the turbulent eddies in the wind, other wave components are generated. During the course of our simulation, these wave modes have much less energy than the dominant wave, and this letter focuses on the growth of the latter. We use k to denote wavenumber, λ for wavelength, a for wave amplitude, ω for wave frequency, c for wave phase velocity, u_* for wind friction velocity, $U_{\lambda/2}$ for the mean wind velocity at a distance of $\lambda/2$ above the wave surface, and c/u_* (and also $c/U_{\lambda/2}$) for wave age. Various cases of different wave ages are simulated, and the growth of the waves provides results for the different evolution stages of ak (cf. Tables I and II). Figure 2 shows the time evolution of the wave steepness based on the wave crest and trough amplitude, a_c and a_t, respectively. The wave nonlinear effect is shown through the difference between $a_c k$ and $a_t k$ [hereafter, we define $a=(a_c+a_t)/2$] and the difference between linear and nonlinear waves. Figure 2 shows that the wave grows fast for young waves with the wave ages $c/u_*=2$ and 5. At $c/u_*=10$ and 14, the wave grows slowly.

TABLE I. Values of α, θ, β, and γ for $c/u_*=2$ at different ak. Values of γ based on the parametrization of Ref. 10, $\gamma=0.17(U_{\lambda/2}/c-1)^2(\omega\rho_a/\rho_w)$, are listed for comparison.

ak	0.05	0.10	0.15	0.20	0.25
α	40.2	36.3	35.1	30.4	26.3
θ	118°	107°	100°	96°	92°
β	36.9	34.6	34.4	30.1	26.3
γ ($\times10^{-3}$)	2.22	2.08	2.07	1.81	1.58
γ ($\times10^{-3}$) [a]	2.23	2.09	1.95	1.80	1.66

[a]Reference 10.

The wind turbulence simulation provides detailed information on the distribution of p_a along the waveform. Figure 3 shows the phase-averaged results of p_a. In Fig. 3(a), we validate our results via comparison with the corresponding case in Ref. 10. In Fig. 3(b), we illustrate the dependence of p_a on the wave steepness. For mild waves (from $ak=0.1$ to 0.15), the magnitude of both the maximum and minimum pressure increases with ak. When the wave becomes steeper (from $ak=0.15$ to 0.20 to 0.25), the pressure maximum increases slightly and moves downstream, while the lower part of the pressure profile changes from a flat shape to a trough. Figure 3(c) shows the dependence of p_a on the wave age. At $c/u_*=2$, the maximum pressure is located downstream of the wave trough. As the wave age increases ($c/u_*=5$), it moves further downstream toward the wave crest. As the wave age increases to $c/u_*=10$, the pressure profile moves upstream. For $c/u_*=14$, the maximum pressure is located on the wave trough.

We next quantify the wave growth rate. Due to the orthogonality of different trigonometric components, for a wave component with the surface elevation $\eta(x,t)=a\cos(kx-\omega t)$, we focus on the corresponding surface pres-

TABLE II. Values of α, θ, β, and γ at $ak=0.1$ with different wave ages.

c/u_*	2	5	10	14
$c/U_{\lambda/2}$	0.12	0.33	0.64	0.86
α	36.3	50.0	27.5	36.2
θ	107°	79°	152°	177°
β	34.6	49.0	17.9	1.62
γ ($\times10^{-3}$)	2.08	1.18	0.215	0.0139

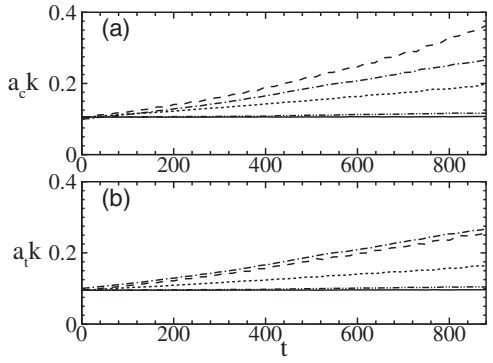

FIG. 2. Evolution of (a) $a_c k$ and (b) $a_t k$: – –, $c/u_*=2$; –·–, $c/u_*=2$ (from linear wave simulation); ···, $c/u_*=5$; –···–, $c/u_*=10$; —, $c/u_*=14$. The time is normalized by $\lambda/U_{\lambda/2}$.

sure component expressed as $p_a(x,t)=\alpha ak\cos(kx-\omega t+\theta)$. Here α denotes the amplitude ratio of the pressure to the wave steepness; and θ denotes the phase difference between the pressure and the waveform (Fig. 3). As in the literature, the wave growth rate parameter β and the fractional rate of energy input γ are defined, respectively, as

$$\beta=(\alpha\sin\theta)/\rho_a u_*^2, \quad \gamma=\omega(\rho_a/\rho_w)(u_*/c)^2\beta. \tag{5}$$

Tables I and II show the dependence of α, θ, β, and γ on ak and c/u_*. The comparison of the γ value with the parametrization by Ref. 10 shows good agreement. The decrease in α as ak increases suggests that the pressure does not simply scale with ak as was assumed in many of the literature. The dependence of β on c/u_* and ak can be understood through the variation in α and θ [Eq. (5)]. Table I shows that when $c/u_*=2$ and ak increases, the variation in θ is small, and β is mainly controlled by α, which decreases as ak increases; the value of γ decreases at the same rate according to Eq. (5).

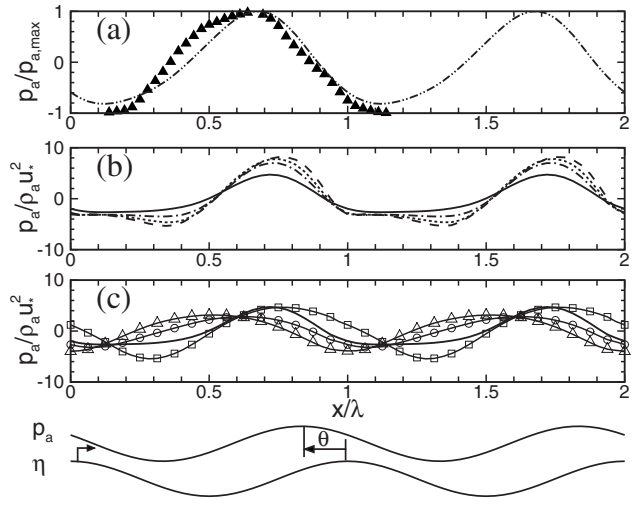

FIG. 3. Surface pressure profiles over monochromatic waves: –···–, ($c/u_*=2$, $ak=0.05$); —, ($c/u_*=2$, $ak=0.1$); –·–, ($c/u_*=2$, $ak=0.15$); ···, ($c/u_*=2$, $ak=0.2$); – –, ($c/u_*=2$, $ak=0.25$); ⊟, ($c/u_*=5$, $ak=0.1$); ⊖, ($c/u_*=10$, $ak=0.1$); △, ($c/u_*=14$, $ak=0.1$). (a) Comparison of simulation result with field measurement data (▲) of Ref. 10; (b) pressure profiles over waves with different steepnesses; (c) pressure profiles over waves with different wave ages. The wind and wave are from left to right. The wave phase is shown in the sketch at the bottom.

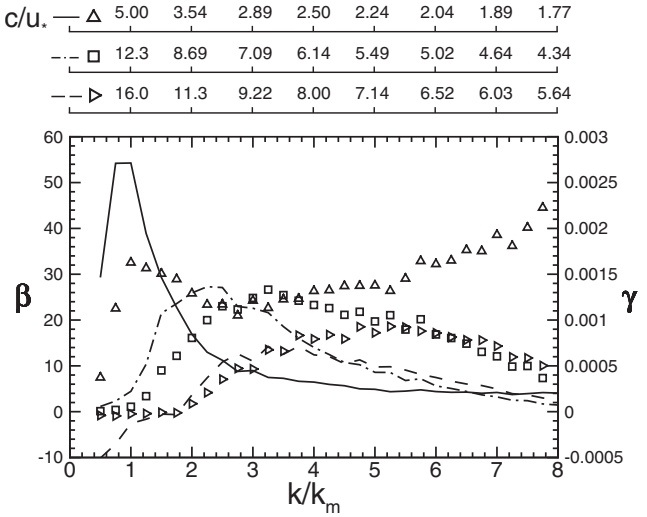

FIG. 4. Values of β (lines) and γ (symbols) for broadband waves: — and △, $c_m/u_*=5$ (case I); –·– and □, $c_m/u_*=12.3$ (case II); – – – and ▷, $c_m/u_*=16$ (case III).

Table II shows that when $ak=0.1$, for different c/u_* cases, the change in β is affected by both α and θ, with the latter determining the efficiency of wind input. As c/u_* increases from 2 to 5, α increases (because the magnitude of the minimum pressure increases as shown in Fig. 3), θ gets closer to 90°, and β becomes larger as a result. As c/u_* further increases to 10 and 14, θ approaches 180°, and β decreases significantly. As c/u_* increases, the variation in β together with the proportionality to $(u_*/c)^2$ [Eq. (5)] makes γ decrease.

We next investigate waves with broadband spectra (Fig. 1). We construct a wavefield based on the wave spectrum obtained during the Joint North Sea Wave Observation Project (JONSWAP) (details are provided in Ref. 15). We consider three cases with different wave ages based on the phase velocity at the peak (denoted by the subscript "m") wavenumber k_m, $c_m/u_*=5$, 12.3, and 16 (the corresponding values of $c_m/U_{\lambda_m/2}$ obtained from the simulations are 0.27, 0.66, and 0.84, respectively), which hereinafter are referred to as cases I, II, and III, respectively.

For the broadband wavefield, it is essential to quantify the wind input for different wave components. At each k, we perform analysis in a way similar to that in the monochromatic wave case [Eq. (5)]. The variation in β and γ with k is shown in Fig. 4. To help understand their behavior, we also indicate the values of c/u_* at different k for the three cases in Fig. 4. Note that according to the wave dispersion relationship, c/u_* decreases as k increases and has different ranges for the three cases. For case I, β reaches its peak around $k=k_m$ and decreases as k further increases; this is consistent with the monochromatic wave case, in which $c/u_*=5$ has a larger value of β than $c/u_*=2$ does. For cases II and III, β first increases with k and reaches its peak around $k=2k_m\sim 4k_m$ (note that in the monochromatic wave case $c/u_*=14$ has smaller value of β than $c/u_*=5$ does), and then decreases as k further increases. For cases II and III, the corresponding c/u_* values of peak β deviate from the value of $c/u_*=5$ shown in the monochromatic wave case, probably

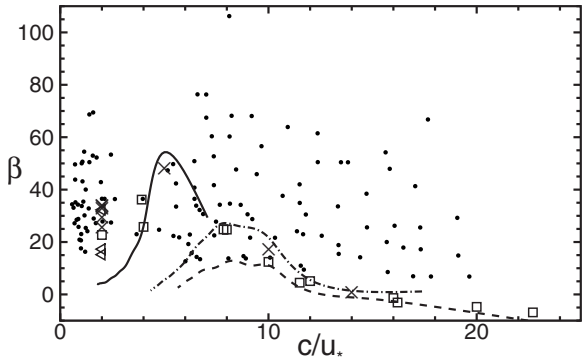

FIG. 5. Wave growth rate parameter β: ●, experimental results compiled in Ref. 7; □, numerical results of Refs. 9 and 11; ◁, numerical results of Ref. 13; ×, current results for monochromatic waves. The lines are the current broadband wave results (see the line legend in Fig. 4).

due to the sheltering effect of dominant waves on relatively short and small waves. At large k, our simulation does not show significant values of β. At these small scales, the pressure induced by the short waves is relatively small compared with the pressure fluctuation in the wind turbulence and is thus difficult to quantify. On the other hand, γ, which measures the fractional rate of wave growth [Eq. (5)], does not reduce as rapidly compared with β (γ even increases with k for case I). In reality, local small waves may grow rapidly to break, serving as an important vehicle for atmosphere-ocean momentum and energy transfer.[16,17]

Figure 5 summarizes our results of β and the comparison with other studies. Our data of monochromatic waves agree with the previous numerical results and (to a less extent) experimental data. As shown by Yang and Shen,[13] many factors, including wave steepness and wind induced surface drift, can affect the value of β (an example for the same $c/u_*=2$ but different wave steepness and surface drift conditions is shown in Fig. 5 using the data of Ref. 13).

Figure 5 shows that for the broadband waves, the long wave components (i.e., the right parts of each curve with relatively large λ and c and thus large c/u_*) have β values close to those from the study of monochromatic waves. This result suggests that for phase-resolved simulation of broadband wavefield using the HOS method, the wind input model for large wave components can be developed based on the analysis of monochromatic waves as a first step of the study. Therefore, it is valuable to have precise laboratory measurement[18] of wind over waves and to perform mechanistic study using numerical simulation. For short waves, as discussed earlier, the mean value of β drops rapidly to have large deviation from the simple wave results, while locally the wind input may have large fluctuations. Therefore, in the HOS method, for wind input to small waves, stochastic modeling is called for. This strategy of deterministic and stochastic wind input modeling for long and short waves, respectively, is consistent with the philosophy of the HOS method.[2,15] Finally, we remark that this study serves as a first step for the modeling of wind input for phase-resolved simulation of nonlinear wavefield. Much more work in the modeling needs to be done. If successful, together with appropriate wave breaking dissipation models, the HOS method can be a useful tool for the study of the nonlinear processes of energy transfer in wind waves. These will be the subjects of our future study.

The support by the ONR through the Young Investigator award to L.S. is gratefully acknowledged. L.S. also wishes to thank Professor Dick K. P. Yue for helpful discussions.

[1]The WISE Group, L. Cavaleri, J.-H.G. M. Alves, F. Ardhuin, A. Babanin, M. Banner, K. Belibassakis, M. Benoit, M. Donelan, J. Groeneweg, T. H. C. Herbers, P. Hwang, P. A. E. M. Janssen, T. Janssen, I. V. Lavrenov, R. Magne, J. Monbaliu, M. Onorato, V. Polnikov, D. Resio, W. E. Rogers, A. Sheremet, J. McKee Smith, H. L. Tolman, G. van Vledder, J. Wolf, and I. Young, "Wave modelling—The state of the art," Prog. Oceanogr. **75**, 603 (2007).
[2]G. Wu, "Direct simulation and deterministic prediction of large-scale nonlinear ocean wave-field," Ph.D. thesis, Massachusetts Institute of Technology, 2004.
[3]D. G. Dommermuth and D. K. P. Yue, "A high-order spectral method for the study of nonlinear gravity waves," J. Fluid Mech. **184**, 267 (1987).
[4]C. C. Mei, M. Stiassnie, and D. K. P. Yue, *Theory and Applications of Ocean Surface Waves. Part 2. Nonlinear Aspects* (World Scientific, Hackensack, NJ, 2005).
[5]M. L. Banner and J.-B. Song, "On determining the onset and strength of breaking for deep water waves. Part II: Influence of wind forcing and surface shear," J. Phys. Oceanogr. **32**, 2559 (2002).
[6]A. V. Babanin, M. L. Banner, I. R. Young, and M. A. Donelan, "Wave-follower field measurements of the wind-input spectral function. Part III: Parametrization of the wind-input enhancement due to wave breaking," J. Phys. Oceanogr. **37**, 2764 (2007).
[7]W. J. Plant, "A relationship between wind stress and wave slope," J. Geophys. Res. **87**, 1961, doi:10.1029/JC087iC03p01961 (1982).
[8]C. Mastenbroek, V. K. Makin, M. H. Garat, and J. P. Giovanangeli, "Experimental evidence of the rapid distortion of turbulence in the air flow over water waves," J. Fluid Mech. **318**, 273 (1996).
[9]P. P. Sullivan, J. C. McWilliams, and C.-H. Moeng, "Simulation of turbulent flow over idealized water waves," J. Fluid Mech. **404**, 47 (2000).
[10]M. A. Donelan, A. V. Babanin, I. R. Young, and M. L. Banner, "Wave-follower field measurements of the wind-input spectral function. Part II: Parametrization of the wind input," J. Phys. Oceanogr. **36**, 1672 (2006).
[11]N. Kihara, H. Hanazaki, T. Mizuya, and H. Ueda, "Relationship between airflow at the critical height and momentum transfer to the traveling waves," Phys. Fluids **19**, 015102 (2007).
[12]S. Yamashita, C. G. Chen, K. Takahashi, and F. Xiao, "Large scale numerical simulations for multi-phase fluid dynamics with moving interfaces," Int. J. Comput. Fluid Dyn. **22**, 405 (2008).
[13]D. Yang and L. Shen, "Direct-simulation-based study of turbulent flow over various waving boundaries," J. Fluid Mech. **650**, 131 (2010).
[14]D. Yang and L. Shen, "Characteristics of coherent vortical structures in turbulent flows over progressive surface waves," Phys. Fluids **21**, 125106 (2009).
[15]D. Yang, "Numerical study of turbulence over various waving boundaries," Ph.D. thesis, Johns Hopkins University, 2010.
[16]W. K. Melville, "The role of surface-wave breaking in air-sea interaction," Annu. Rev. Fluid Mech. **28**, 279 (1996).
[17]J. H. Duncan, "Spilling breakers," Annu. Rev. Fluid Mech. **33**, 519 (2001).
[18]M. A. Donelan and W. J. Plant, "A threshold for wind-wave growth," J. Geophys. Res. **114**, C07012, doi:10.1029/2008JC005238 (2009).